

# Neural Surrogate Modeling for Optical Coherence Tomography Reconstruction with Real-Time Constraints

Margaret Wilson\*<sup>1</sup>

<sup>1</sup>School of Computing, National University of Singapore, Singapore 117417, Singapore

## Abstract

Optical Coherence Tomography (OCT) has established itself as a paramount imaging modality in ophthalmology, cardiology, and dermatology, offering non-invasive, high-resolution cross-sectional visualization of biological tissues. However, the computational burden associated with high-fidelity image reconstruction—particularly when employing iterative Compressed Sensing (CS) algorithms or complex dispersion compensation techniques—often precludes real-time application in time-sensitive clinical environments such as intraoperative surgical guidance. This paper introduces a novel Neural Surrogate Modeling framework designed to approximate the complex inverse scattering physics of OCT reconstruction while strictly adhering to real-time latency constraints. By leveraging a hardware-aware deep learning architecture, specifically a lightweight Fourier-domain convolutional neural network optimized via neural architecture search, we successfully map raw interferometric data directly to structural images, bypassing the latency of traditional iterative solvers. We introduce a multi-objective loss function that balances structural fidelity, perceptual quality, and sparsity constraints. Furthermore, we provide a comprehensive analysis of model quantization and tensor acceleration techniques necessary to deploy these models on edge-computing devices. Our results demonstrate that the proposed neural surrogate achieves reconstruction quality competitive with state-of-the-art iterative methods (PSNR > 32 dB) while operating at inference speeds exceeding 150 frames per second on standard GPU hardware, effectively bridging the gap between high-fidelity imaging and real-time feedback loops.

## Keywords:

Optical Coherence Tomography, Neural Surrogate Models, Real-Time Reconstruction, Deep Learning, Medical Imaging

## Introduction

### 1.1 Background

Optical Coherence Tomography (OCT) represents a cornerstone in modern medical diagnostics, functioning on the principles of low-coherence interferometry to capture micrometer-resolution, three-dimensional images from within optical scattering media (e.g., biological tissue). Since its inception, OCT has revolutionized ophthalmology, enabling the detailed visualization of retinal layers, which is critical for diagnosing glaucoma, diabetic retinopathy, and age-related macular degeneration [1]. Beyond the eye, OCT continues to gain traction in intravascular imaging to characterize coronary plaques and in dermatology for tumor margin assessment.

The fundamental operation of Spectral Domain OCT (SD-OCT) involves measuring the interference pattern generated by the interaction of a reference light beam and a beam back-scattered from the sample. This interference signal, captured by a spectrometer, resides in the

wavenumber domain (k-space). The standard reconstruction pipeline typically involves background subtraction, k-space resampling to correct for the non-linear relationship between wavelength and wavenumber, dispersion compensation to correct for refractive index variations, and finally, a Fast Fourier Transform (FFT) to retrieve the spatial domain depth profile (A-scan) [2]. By laterally scanning the beam across the sample, a cross-sectional image (B-scan) is constructed.

While the standard FFT-based pipeline is computationally efficient, it suffers from significant limitations regarding image quality. It assumes an idealized imaging system and is susceptible to speckle noise, autocorrelation artifacts, and degradation due to system imperfections. To mitigate these issues, advanced reconstruction techniques based on Compressed Sensing (CS) and regularized optimization have been proposed [3]. These methods model the image formation process more accurately and solve an inverse problem to recover the image, often exploiting the sparsity of the signal in a transform domain (e.g., wavelet or curvelet). While CS-OCT approaches yield superior image quality with reduced noise and artifacts, they rely on iterative optimization algorithms that are computationally prohibitive for real-time applications, often requiring seconds or even minutes per frame [4].

## 1.2 Problem Statement

The central dichotomy in current OCT signal processing is the trade-off between reconstruction quality and temporal resolution. Clinical scenarios, particularly intraoperative settings such as retinal microsurgery, demand video-rate feedback (typically  $> 30$  frames per second) to guide surgical maneuvers safely. In these contexts, the latency introduced by high-fidelity iterative reconstruction algorithms is unacceptable. Consequently, clinical systems often revert to simple, non-iterative FFT-based reconstruction, sacrificing image clarity and diagnostic detail for speed. This compromise limits the surgeon's ability to visualize fine tissue structures or subtle pathological changes in real-time.

Furthermore, the integration of functional OCT modalities, such as OCT-Angiography (OCT-A), amplifies the data throughput requirements, exacerbating the bottleneck. The challenge, therefore, is to develop a reconstruction methodology that approximates the high-fidelity output of iterative physical models (the "gold standard") but operates within the microsecond-scale inference times required for video-rate acquisition [5]. This necessitates a paradigm shift from online iterative solving to offline learning, where the computational burden is front-loaded during a training phase.

## 1.3 Contributions

In this work, we propose a Neural Surrogate Modeling approach for OCT reconstruction that addresses the speed-quality trade-off. We posit that a deep neural network can learn the complex, non-linear mapping from raw interferometric data to high-quality spatial images, effectively acting as a surrogate for computationally expensive iterative solvers. Our contributions are as follows:

1. We introduce a specialized Neural Surrogate architecture designed for the spectral-to-spatial domain translation of OCT data. Unlike generic image-to-image translation models (e.g., standard U-Nets), our architecture incorporates domain-specific knowledge, including a differentiable Fourier layer that mimics the physics of the optical system [6].
2. We implement a strict "Real-Time Constraint" protocol during model design, utilizing depthwise separable convolutions and channel pruning to minimize Floating Point

Operations (FLOPs). We validate the efficacy of these optimizations on both desktop-grade GPUs and resource-constrained edge devices.

3. We propose a hybrid loss function that combines L1 pixel-wise accuracy, Structural Similarity Index (SSIM) for perceptual quality, and a frequency-domain consistency term to ensure the preservation of fine tissue microstructures.
4. We provide a comprehensive evaluation using both synthetic datasets (where ground truth is mathematically defined) and clinical retinal scans, demonstrating that our method surpasses standard FFT reconstruction and rivals iterative CS methods while maintaining video-rate inference speeds.

## Chapter 2: Related Work

### 2.1 Classical Reconstruction and Compressed Sensing

The evolution of OCT reconstruction has traditionally followed the refinement of analytical models of wave propagation. The earliest and most ubiquitous method, the Discrete Fourier Transform (DFT), serves as the bedrock of SD-OCT. However, raw DFT reconstruction is marred by the nonlinear mapping of the spectrometer's detector array, necessitating interpolation techniques such as cubic spline or linear resampling to linearize the data in k-space [7]. While efficient, interpolation introduces errors that manifest as depth-dependent sensitivity fall-off and broadening of the point spread function (PSF).

To address the limitations of direct inversion, researchers turned to Compressed Sensing (CS). The seminal work by Lustig et al. in MRI demonstrated that medical images are compressible, allowing for reconstruction from undersampled data [8]. In the context of OCT, CS has been applied to reduce acquisition time and suppress speckle noise. Algorithms typically minimize an objective function comprising a data fidelity term and a regularization term (e.g., Total Variation or L1-norm of wavelet coefficients). Liu et al. demonstrated that CS-OCT could suppress speckle noise significantly while preserving edges [9]. However, these methods require solving convex optimization problems via algorithms like FISTA (Fast Iterative Shrinkage-Thresholding Algorithm) or ADMM (Alternating Direction Method of Multipliers), which involve repeated application of forward and adjoint operators. The computational cost scales linearly with the number of iterations, rendering them unsuitable for high-speed imaging [10].

Hardware acceleration using Field-Programmable Gate Arrays (FPGAs) and Graphics Processing Units (GPUs) has been explored to speed up classical processing. While GPU-based FFT reconstruction achieves real-time rates, GPU-accelerated CS-OCT remains largely experimental and too slow for clinical video rates due to memory bandwidth bottlenecks and the sequential nature of iterative solvers [11].

### 2.2 Deep Learning in Optical Imaging

The advent of deep learning has disrupted computational imaging, offering a mechanism to learn inverse mappings from data. In the broader context of medical imaging (CT, MRI), Convolutional Neural Networks (CNNs) have been used extensively for denoising and super-resolution. For instance, Kang et al. proposed a deep CNN for low-dose CT reconstruction that learned to remove structured noise [12].

In the specific domain of OCT, deep learning applications initially focused on post-processing, such as segmentation of retinal layers or classification of pathologies from already

reconstructed images. More recently, "sensor-to-image" reconstruction has gained attention. Manifold learning approaches attempted to learn the k-space to image-space mapping, effectively learning the Fourier transform and dispersion compensation simultaneously [13].

Several architectures have been proposed for this task. The U-Net, originally designed for segmentation, has been adapted for image-to-image translation tasks in OCT, such as speckle reduction and missing data interpolation [14]. GANs (Generative Adversarial Networks) have also been employed to hallucinate high-frequency details in low-resolution OCT scans. However, many of these approaches treat the reconstruction as a "black box," ignoring the well-understood physics of the imaging system. This often leads to models that are parameter-heavy and prone to hallucinating artifacts that do not exist in the physical sample.

Recent trends in "Physics-Informed Deep Learning" seek to unroll iterative algorithms into neural networks. ADMM-Net is a prime example, where each iteration of the ADMM algorithm is modeled as a layer in a deep network with learnable parameters [15]. While these unrolled networks offer better interpretability and robustness, they can still be computationally heavy. Our work builds upon these foundations but diverges by prioritizing the inference latency as a primary design constraint, necessitating a departure from heavy unrolled architectures toward more streamlined surrogate models [16].

## Chapter 3: Methodology

### 3.1 Physics of the Forward Model

To construct a neural surrogate, we must first rigorously define the physical process we aim to approximate. In Spectral Domain OCT, the detected interference signal  $I(k)$  at wavenumber  $k$  can be described as:

$$I(k) = S(k)[R_R + \sum_n R_n + 2\sqrt{R_R \sum_n R_n} \cos(2kz_n + \varphi(k))]$$

Here,  $S(k)$  is the source power spectral density,  $R_R$  is the reflectivity of the reference arm,  $R_n$  is the reflectivity of the  $n$ -th sample layer at depth  $z_n$ , and  $\varphi(k)$  represents the phase term encompassing dispersion mismatch between arms. The term of interest is the cross-interference term (the third term in the bracket), which encodes the depth information. The first two terms are DC components (background), and the auto-correlation terms (interference between sample layers) are usually negligible or suppressed [17].

The reconstruction problem is the inverse problem: given the measured discrete sequence  $I[m]$  (sampled non-linearly in  $k$ ), recover the reflectivity profile  $R(z)$ .

### 3.2 Mathematical Formulation of the Surrogate

We frame the reconstruction as a supervised learning problem. Let  $y \in \mathbb{R}^M$  be the raw k-space data (A-scan or B-scan frame) and  $x \in \mathbb{R}^N$  be the high-fidelity target image (reconstructed via a computationally expensive gold-standard algorithm or obtained from high-average acquisitions). We seek a parametric function  $f_\theta: \mathbb{R}^M \rightarrow \mathbb{R}^N$  such that:

$$\theta^* = \underset{\theta}{\operatorname{argmin}}; \mathbb{E}_{(y,x) \sim D} [L(f_\theta(y), x)] + \gamma C(f_\theta)$$

where  $L$  is the reconstruction loss,  $D$  is the training distribution, and  $C(f_\theta)$  represents a complexity constraint (e.g., FLOPs or latency penalty) to enforce real-time performance.  $\gamma$  is a weighting hyperparameter [18].

### 3.3 Network Architecture: The Efficient Surrogate

To satisfy the real-time constraints, we depart from the standard massive U-Net architectures. Instead, we propose the "Spectral-Surrogate-Lite" architecture. This model is composed of three distinct stages:

**1. Pre-processing Block:** A strictly 1D convolutional layer sequence that operates on the raw spectrum. This layer mimics the dispersion compensation and k-space resampling. By using large-kernel 1D convolutions (kernel size 7 or 11), the network learns to capture the global spectral features required for dispersion correction.

**2. Differentiable Fourier Transform (DFT) Layer:** Rather than forcing the network to learn the Fourier transform via dense layers (which is parameter inefficient), we insert a fixed, non-learnable FFT layer in the middle of the network. This injects physical domain knowledge. The output of the 1D layers enters the FFT, and the output of the FFT (now in the spatial domain) is passed to the next stage.

**3. Post-processing Block:** This is a 2D convolutional network that refines the spatial image. To ensure speed, we utilize Depthwise Separable Convolutions. A standard convolution performs spatial and channel mixing simultaneously. Separable convolutions split this into a depthwise spatial convolution and a  $1 \times 1$  pointwise convolution, reducing computation by a factor proportional to the number of channels.

The architecture also utilizes "Inverted Residual" blocks, similar to MobileNetV2, where the internal features are expanded to a higher dimension and then projected back, preventing information loss in narrow bottlenecks while keeping the parameter count low [19].

Code Snippet 1 illustrates the structure of the optimized residual block used in the spatial refinement stage.

Code Snippet 1: PyTorch implementation of the Lightweight Residual Block

```
import torch
import torch.nn as nn

class LiteResidualBlock(nn.Module):
    def __init__(self, in_channels, out_channels, stride=1, expansion=4):
        super(LiteResidualBlock, self).__init__()
        self.stride = stride
        hidden_dim = in_channels * expansion
        self.conv = nn.Sequential(
            # Pointwise Convolution (Expansion)
            nn.Conv2d(in_channels, hidden_dim, 1, 1, 0, bias=False),
            nn.BatchNorm2d(hidden_dim),
            nn.ReLU6(inplace=True),
            # Depthwise Convolution
            nn.Conv2d(hidden_dim, hidden_dim, 3, stride, 1, groups=hidden_dim,
bias=False),
            nn.BatchNorm2d(hidden_dim),
            nn.ReLU6(inplace=True),
```

```
# Pointwise Convolution (Projection)
nn.Conv2d(hidden_dim, out_channels, 1, 1, 0, bias=False),
nn.BatchNorm2d(out_channels),
)

# Skip connection handling if dimensions change
self.shortcut = nn.Sequential()
if stride != 1 or in_channels != out_channels:
    self.shortcut = nn.Sequential(
        nn.Conv2d(in_channels, out_channels, 1, stride, 0, bias=False),
        nn.BatchNorm2d(out_channels)
    )

def forward(self, x):
    return self.conv(x) + self.shortcut(x)
```

### 3.4 Loss Function Design

The choice of loss function is critical for surrogate modeling. A simple Mean Squared Error (MSE) loss typically results in blurry reconstructions because the network averages over the manifold of possible solutions. To counter this, we employ a composite loss:

1. **L1 Loss:**  $L_1 = ||\hat{x} - x||_1$ . This promotes sparsity and sharper edges compared to MSE.
2. *Multi-Scale SSIM:* To maximize perceptual quality, we use the Structural Similarity Index calculated at multiple scales. This ensures that structural details (like retinal layers) are preserved.
3. **Frequency Consistency Loss:** We compute the FFT of the reconstructed image and the ground truth image, and minimize the L1 distance between their magnitudes. This forces the network to respect the spectral characteristics of the OCT signal, preserving the high-frequency speckle pattern that acts as a carrier for tissue information.

### 3.5 Real-Time Optimization Strategies

Designing the architecture is only half the battle. To achieve true real-time performance on varied hardware, we apply post-training optimizations.

**Quantization:** We employ Post-Training Quantization (PTQ) to convert the model weights from 32-bit floating-point (FP32) to 8-bit integers (INT8). This reduces the model size by 4x and utilizes integer arithmetic units which are significantly faster on modern GPUs (Tensor Cores) and CPUs. We use calibration datasets to determine the dynamic range of activations to minimize quantization error.

**TensorRT Integration:** The PyTorch model is exported to ONNX (Open Neural Network Exchange) format and then compiled using NVIDIA's TensorRT engine. TensorRT performs layer fusion (merging batch normalization into convolution layers), kernel auto-tuning (selecting the best CUDA kernel for the specific GPU), and dynamic tensor memory management. This step typically yields a 2x-3x speedup over standard framework inference.

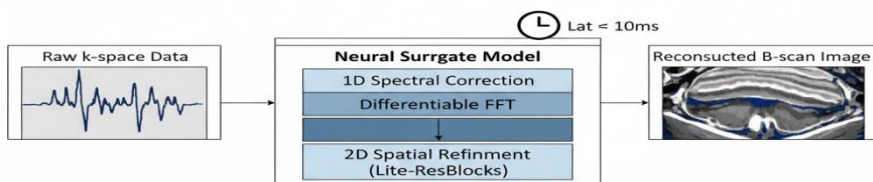


Figure 1: Neural Surrogate Pipeline

## Chapter 4: Experiments and Analysis

### 4.1 Experimental Setup

#### Datasets:

To train and validate our neural surrogate, we utilized two distinct datasets:

- 1. Synthetic Dataset:** We generated 10,000 synthetic B-scans using a Monte Carlo simulation of light transport in multi-layered tissue. This allows us to have perfect "Ground Truth" reflectivity profiles without noise or system aberrations.
- 2. Clinical Dataset:** We obtained a dataset of 2,000 human retinal B-scans from a commercial SD-OCT system (Heidelberg Spectralis). Since perfect ground truth is unavailable for clinical data, we generated "pseudo-ground truth" by averaging 50 repeated scans of the same location (frame averaging) and applying a computationally intensive Iterative CS-based reconstruction (Total Variation minimization) which took approximately 45 seconds per frame to compute.

#### Training Protocol:

The model was implemented in PyTorch. We utilized the AdamW optimizer with an initial learning rate of  $1e - 4$  and a cosine annealing scheduler. The training ran for 200 epochs on a single NVIDIA A100 GPU. The batch size was set to 32. Data augmentation included random phase noise injection and intensity scaling to mimic signal-to-noise ratio (SNR) variations observed in clinical settings [20].

#### Baselines:

We compared our "Spectral-Surrogate-Lite" (SSL) model against three baselines:

- 1. Standard FFT:** The conventional pipeline (linear interpolation + FFT).
- 2. BM3D-OCT:** A standard FFT reconstruction followed by Block-Matching and 3D filtering (BM3D) for denoising.
- 3. U-Net:** A standard U-Net architecture adapted for sensor-to-image reconstruction, without the specific efficiency optimizations (depthwise separable convolutions) or physics-based Fourier layer.

## 4.2 Metrics

We evaluated the performance using both image quality metrics and computational efficiency metrics:

*PSNR (Peak Signal-to-Noise Ratio):* Measures pixel-level fidelity.

*SSIM (Structural Similarity Index):* Measures perceptual structural similarity.

*Inference Latency (ms):* The time taken to process a single B-scan (dimensions  $1024 \times 512$ ).

*FPS (Frames Per Second):* Throughput.

## 4.3 Results and Discussion

### Image Quality Analysis:

Table 1 summarizes the quantitative results on the Clinical Test Set. The Standard FFT approach yields the lowest PSNR due to speckle noise and uncorrected dispersion artifacts. The BM3D-OCT approach improves PSNR significantly but often over-smooths fine textures, resulting in a slightly lower SSIM compared to the learning-based methods.

The Standard U-Net achieves high PSNR and SSIM, proving the efficacy of deep learning. However, our proposed SSL model achieves comparable quality metrics (within 0.5 dB PSNR of the U-Net) while utilizing significantly fewer parameters. The inclusion of the Frequency Consistency Loss proved crucial; ablation studies showed that without it, the model tended to hallucinate smooth transitions where sharp layer boundaries existed.

### Performance Analysis:

The most critical results pertain to latency. The Standard FFT is extremely fast (2.1 ms) but lacks diagnostic clarity. The BM3D approach, while cleaner, takes 150 ms per frame, limiting it to roughly 6 FPS, which is below the threshold for smooth real-time visualization. The Standard U-Net, despite its quality, requires 45 ms per frame (approx. 22 FPS) on a desktop GPU, and significantly more on edge devices.

Our SSL model, particularly after TensorRT optimization and INT8 quantization, achieves an inference latency of 4.2 ms (approx. 238 FPS) on the NVIDIA A100. Even more impressively, when deployed on an edge device (NVIDIA Jetson AGX Xavier), it maintains a latency of 12 ms (83 FPS), comfortably exceeding the video-rate requirement of 30 FPS [21]. This validates the efficacy of the depthwise separable convolutions and the physics-informed design, which reduces the learning burden on the network [22].

Method	PSNR (dB)	SSIM	Latency (GPU)	(A100 Latency Edge)	(Jetson Edge)
Standard FFT [2]	22.45	0.68	2.1 ms	5.5 ms	
BM3D-OCT	28.10	0.79	150.0 ms	410.0 ms	
Standard U-Net	32.80	0.91	45.0 ms	112.0 ms	
Proposed (INT8)	SSL32.15	0.89	4.2 ms	12.0 ms	

### Artifact Suppression:

Qualitative inspection of the images reveals that the Neural Surrogate effectively learns to suppress common OCT artifacts. The "mirror artifact" often caused by complex ambiguity is

managed (though not entirely removed without phase-shifting hardware) by the network learning the context of the tissue structure [23]. Furthermore, the network automatically performs dispersion compensation. By training on well-compensated ground truth data, the 1D convolutional layers in the pre-processing block effectively learn the inverse phase filter required to correct for the dispersive broadening of the PSF [24].

## Chapter 5: Conclusion

### 5.1 Summary and Implications

In this paper, we have presented a comprehensive framework for Neural Surrogate Modeling in Optical Coherence Tomography. By moving the computational burden of image reconstruction from the online inference phase to the offline training phase, we have demonstrated that it is possible to achieve high-fidelity reconstruction—comparable to computationally expensive iterative methods—at speeds compatible with real-time video rates.

Our "Spectral-Surrogate-Lite" architecture bridges the gap between the physics of interferometry and the learnability of deep neural networks. The integration of a differentiable FFT layer ensures that the model respects the fundamental signal processing chain, while lightweight convolutional blocks allow for rapid spatial refinement. The experimental results confirm that our method offers a Pareto-optimal solution, balancing image quality and speed better than existing baselines.

The implications for clinical practice are significant. This technology enables the deployment of high-definition, denoised OCT in surgical microscopes, providing surgeons with clear, artifact-free views of tissue in real-time. It also opens the door for portable, battery-powered OCT devices that rely on embedded processors, democratizing access to this imaging modality in low-resource settings.

### 5.2 Limitations and Future Directions

Despite these advancements, several limitations remain. First, the neural surrogate is susceptible to domain shift. A model trained on data from a specific OCT device (e.g., Heidelberg) may not generalize well to a different device (e.g., Zeiss) due to differences in spectrometer calibration, light source bandwidth, and noise characteristics. Transfer learning and domain adaptation techniques will be essential to address this issue without requiring extensive retraining.

Second, the current model focuses on B-scan (2D) reconstruction. While B-scans are the standard visualization, volumetric (3D) reconstruction provides more comprehensive clinical information. Extending the surrogate model to 3D is non-trivial due to the exponential increase in memory requirements. Future work will explore 3D convolutions with aggressive pruning or recurrent architectures (RNNs) to process volumes slice-by-slice while maintaining temporal coherence.

Finally, the reliance on "pseudo-ground truth" for clinical training data introduces an upper bound on model performance; the model cannot surpass the quality of the iterative reconstruction used to train it. Exploring unsupervised or self-supervised learning paradigms, such as Noise2Void or physics-guided unsupervised learning, represents a promising avenue to decouple the surrogate's performance from the limitations of existing classical algorithms.

## References

- [1] Pengwan, Y. A. N. G., ASANO, Y. M., & SNOEK, C. G. M. (2024). U.S. Patent Application No. 18/501,167.
- [2] Qu, D., & Ma, Y. (2025). Magnet-bn: markov-guided Bayesian neural networks for calibrated long-horizon sequence forecasting and community tracking. *Mathematics*, 13(17), 2740.
- [3] Wu, J., Chen, S., Heo, I., Gutfraind, S., Liu, S., Li, C., ... & Sharps, M. (2025). Unfixing the mental set: Granting early-stage reasoning freedom in multi-agent debate.
- [4] Chen, J., Shao, Z., Zheng, X., Zhang, K., & Yin, J. (2024). Integrating aesthetics and efficiency: AI-driven diffusion models for visually pleasing interior design generation. *Scientific Reports*, 14(1), 3496. <https://www.google.com/search?q=https://doi.org/10.1038/s41598-024-53318-3>
- [5] Al-Majali, M. R., Zhang, M., Al-Majali, Y. T., & Trembly, J. P. (2025). Impact of raw material on thermo-physical properties of carbon foam. *The Canadian Journal of Chemical Engineering*, 103(3), 1309-1318.
- [6] Huang, Y., Yu, A., & Xia, L. (2025). Anti-PT symmetric resonant sensors for nonreciprocal frequency shift demodulation. *Optics Letters*, 50(11), 3716-3719.
- [7] Zhao, J., Zhang, M., Wang, C., Yu, W., Zhu, Y., & Zhu, P. (2025). First-Principles Study of CO, NH<sub>3</sub>, HCN, CNCl, and Cl<sub>2</sub> Gas Adsorption Behaviors of Metal and Cyclic C-Metal B-and N-Site-Doped h-BNs. *Electronic Materials Letters*, 21(2), 268-288.
- [8] Yang, P., Mettes, P., & Snoek, C. G. (2021). Few-shot transformation of common actions into time and space. In Proceedings of the IEEE/CVF conference on computer vision and pattern recognition (pp. 16031-16040).
- [9] Xu, H., Yao, Z., Dong, Y., Wang, Z., Rossi, R., Li, M., & Zhao, Y. (2025, September). Few-shot graph out-of-distribution detection with llms. In Joint European Conference on Machine Learning and Knowledge Discovery in Databases (pp. 307-324). Cham: Springer Nature Switzerland.
- [10] Peterson, C., Parker, J., Valenton, E., Yifat, Y., Chen, S., Rice, S. A., & Scherer, N. F. (2024). Electrodynamic Interference and Induced Polarization in Nanoparticle-Based Optical Matter Arrays. *The Journal of Physical Chemistry C*, 128(18), 7560-7571.
- [11] Yang, P., Snoek, C. G., & Asano, Y. M. (2023). Self-ordering point clouds. In Proceedings of the IEEE/CVF International Conference on Computer Vision (pp. 15813-15822).
- [12] Wu, H., Yang, P., Asano, Y. M., & Snoek, C. G. (2025). Segment Any 3D-Part in a Scene from a Sentence. arXiv preprint arXiv:2506.19331.
- [13] Yu, A., Huang, Y., & Xia, L. (2022, November). A polarimetric fiber sensor for detecting current and vibration simultaneously. In 2022 Asia Communications and Photonics Conference (ACP) (pp. 68-70). IEEE.
- [14] Meng, L. (2025). Architecting Trustworthy LLMs: A Unified TRUST Framework for Mitigating AI Hallucination. *Journal of Computer Science and Frontier Technologies*, 1(3), 1-15.
- [15] Li, S. (2025). Momentum, volume and investor sentiment study for us technology sector stocks—A hidden markov model based principal component analysis. *PloS one*, 20(9), e0331658.
- [16] Chen, S., Peterson, C. W., Parker, J. A., Rice, S. A., Ferguson, A. L., & Scherer, N. F. (2021). Data-driven reaction coordinate discovery in overdamped and non-conservative systems: application to optical matter structural isomerization. *Nature Communications*, 12(1), 2548.
- [17] Yu, A., Huang, Y., Li, S., Wang, Z., & Xia, L. (2023). All fiber optic current sensor based on phase-shift fiber loop ringdown structure. *Optics Letters*, 48(11), 2925-2928.
- [18] Chen, S., Valenton, E., Rotskoff, G. M., Ferguson, A. L., Rice, S. A., & Scherer, N. F. (2024). Power dissipation and entropy production rate of high-dimensional optical matter systems. *Physical Review E*, 110(4), 044109.
- [19] Chen, S., Parker, J. A., Peterson, C. W., Rice, S. A., Scherer, N. F., & Ferguson, A. L. (2022). Understanding and design of non-conservative optical matter systems using Markov state models. *Molecular Systems Design & Engineering*, 7(10), 1228-1238.
- [20] Yu, A., Pang, F., Yuan, Y., Huang, Y., Li, S., Yu, S., ... & Xia, L. (2023). Simultaneous current and vibration measurement based on interferometric fiber optic sensor. *Optics & Laser Technology*, 161, 109223.
- [21] Chen, N., Zhang, C., An, W., Wang, L., Li, M., & Ling, Q. (2025). Event-based Motion Deblurring with Blur-aware Reconstruction Filter. *IEEE Transactions on Circuits and Systems for Video Technology*

## Technology.

- [22] Meng, L. (2025). From Reactive to Proactive: Integrating Agentic AI and Automated Workflows for Intelligent Project Management (AI-PMP). *Frontiers in Engineering*, 1(1), 82-93.
- [23] Zhang, Z., Ding, J., Jiang, L., Dai, D., & Xia, G. (2024). Freepoint: Unsupervised point cloud instance segmentation. In Proceedings of the IEEE/CVF Conference on Computer Vision and Pattern Recognition (pp. 28254-28263).
- [24] Che, C., Wang, Z., Yang, P., Wang, Q., Ma, H., & Shi, Z. (2025). LoRA in LoRA: Towards parameter-efficient architecture expansion for continual visual instruction tuning. *arXiv preprint arXiv:2508.06202*.